https://doi.org/10.5194/nhess-2019-263
Preprint. Discussion started: 26 August 2019

Natural Hazards and Earth System Sciences
Discussions

Investigating beach erosion related with its recovery at Phra Thong Island, Thailand caused by the 2004 Indian Ocean tsunami

Ryota Masaya [1], Anawat Suppasri [2], Kei Yamashita [2], Fumihiko Imamura [2], Chris Gouramanis [3] and Natt Leelawat [4, 5]

[1]Graduate School of Engineering, Tohoku University, Aoba-yama 6-6-06, Aoba-ku, Sendai 980-0845, Japan
[2]International Research Institute of Disaster Science, Tohoku University, 468-1 Aoba, Aramaki-Aza, Aoba-ku, Sendai 980-0845, Japan
[3]Department of Geography, National University of Singapore, 10 Kent Ridge Crescent, Singapore 119260, Singapore
[4]Department of Industrial Engineering, Faculty of Engineering, Chulalongkorn University, Phayathai Road, Pathumwan, Bangkok 10330, Thailand
[5]Disaster and Risk Management Information Systems Research Group, Chulalongkorn University, Phayathai Road, Pathumwan, Bangkok 10330, Thailand
*Corresponding author.
E-mail address: ryota.masaya.r6@dc.tohoku.ac.jp (Ryota Masaya)

Abstract

The 2004 Indian Ocean Tsunami and the 2011 Great East Japan earthquake and tsunami caused large-scale topographic changes in coastal areas. Whereas much research has focused on coastlines that have or had large human populations, little focus has been paid on coastlines that have little or no infrastructure. The importance of examining erosional and depositional mechanisms of tsunami events lies in the rapid reorganisation that coastlines must undertake immediately after an event. Through understanding the precursor conditions to this reorganisation is paramount to the reconstruction of the coastal environment. This study examines the locations of sediment erosion and deposition during the 2004 Indian Ocean Tsunami event on the relatively pristine Phra Thong Island, Thailand. Coupled with satellite imagery, we use numerical simulations and sediment transportation models to determine the locations of significant erosion and the areas where much of that sediment was redeposited during the tsunami inundation and backwash processes. Our modelling approach confirms that beaches on Phra Thong Island were significantly eroded by the 2004 tsunami, predominantly during the backwash phase of the first and largest wave to strike the island. Although 2004 tsunami sediment deposits are found on the island, we demonstrate that most of the sediment was deposited in the shallow coastal area, facilitating quick recovery of the beach when normal coastal processes resume.

1. Introduction

The 2004 Indian Ocean Tsunami and the 2011 Great East Japan earthquake and tsunami caused large-scale topographic changes in coastal areas (Pari et al., 2008; Goto et al., 2011a; Tanaka et al., 2011; Haraguchi et al., 2012; Hirao et al., 2012; Udo et al., 2013; Imai et al., 2015). Since the two tsunami events, long-term topographic changes ranging from years to over a decade have been confirmed in areas affected by the two events (Choowong et al., 2009; Ali et al., 2015; Udo et al., 2016; Mieda et al., 2017; Koiwa et al., 2018), but knowledge regarding the processes of topographic recovery remain poorly understood. Long-term topographic changes in the coastal area have not considered the perspective of early restoration and reconstruction in areas affected by the 2011 tsunami. Structural measures, such as levee construction are moving forward, creating the potential for future problems. Coastal areas that have undergone large-scale topographic changes in a tsunami do not necessarily return to their original topographies. In cases where topographic changes continue without recovery (Udo et al., 2016; Koiwa et al., 2018), it is important to take structural measures that consider future topographic scenarios.

Because reconstruction plans must be formulated in a short time after the tsunami while recovery may take several years, it is difficult to predict the recovery process of coastal areas from field surveys and reflect this in structural measures. It is therefore necessary to clarify in advance the response mechanism as to how the coastal area will recover from large-scale topographic changes caused by a tsunami. To clarify the response mechanism of tsunami-affected topography requires a thorough understanding of the sediment budget in the sedimentary system after the event. Defining the conditions of sediment transport during the tsunami is also key for the initial response process.

Prior studies have mainly estimated sediment transport conditions, such as erosion and sediment deposition through remote sensing(e.g. Fagherazzi & Du 2008, Choowong et al 2009; Liew et al 2010), and sedimentological and stratigraphic analysis (e.g. Paris et al 2007; Hawkes et al 2007; Switzer et al 2012); however, the information obtained regarding the final results of the sediment transport process is limited. It is difficult to obtain information on where sediment has eroded and deposited and whether topographic changes caused by the local sediment runoff or deposition are the results of action from inflow or backwash (e.g. Pham et al 2018). This information determines the sediment budget in the system before and after the tsunami and is therefore important for considering topographic recovery. Therefore, in addition to information from remote sensing and sedimentological data, analyzing numerical simulation results to reproduce spatial-temporal phenomena is effective when discussing the sediment transport process. In recent years, the movable bed model for simulating tsunami sediment transport has been developed, improved, and applied in the field (Takahashi et al., 1999; Takahashi et al., 2008; Takahashi et al., 2011; Takahashi et al., 2012; Morishita et al., 2014; Yamashita et al., 2015; Arimitsu et al., 2017; Yamashita et al., 2018), and reproducibility has been confirmed by comparison between the calculated and measured values.

An important consideration in the recovery process following catastrophic marine events (e.g. typhoon and tsunami) is the degree of development and human modification of the coastal zone prior to the event. Artificial structures, such as sea walls, roads and buildings interfere with overwash processes, and these areas are often targeted from reconstruction and rehabilitation through rapid engineering reconstruction. Little is known about the recovery processes in sparsely developed and populated areas, and Phra Thong Island, western Thailand is an ideal location to examine the recovery processes following a major tsunami event.

Examining the sediment transport processes on Phra Thong Island is expected to elucidate phenomena, improve numerical calculation models for the future and is applicable to other areas. Furthermore, many palaetsunami deposits were identified in areas impacted by the 2004 IOT on Phra Thong Island (Jankaew et al., 2008; Sawai et al., 2009; Fujino et al., 2009; Fujino et al., 2010; Brill et al., 2012a, b; Pham et al., 2017; Gouramanis et al., 2017). Thus, clarifying the sediment transport conditions of the 2004 tsunami will be important for future estimations of history, scope and cause of older tsunamis in Indian Ocean coastal areas.

This study investigates the conditions of sediment transport and considers the factors involved in early recovery of the Phra Thong Island beaches after the 2004 tsunami. We used tsunami sediment transport calculations to spatio-temporally reproduce the sediment transport processes occurring during the tsunami.

2. Conditions and method

2.1. *Phra Thong Island, Thailand*

During the 2004 Indian Ocean tsunami, a wave exceeding 20 m at its highest was observed at the southernmost tip of Phra Thong Island (Fig. 1). Over 70 people were lost and a village of 100 households disappeared. Geomorphologically, the western coast of the island has a beach ridge sequence trending parallel to the coast, which formed during the sea level regression following mid-Holocene sea level highstand at *ca.* 6,000 years ago (Brill et al. 2015). The eastern shore of the island is extensively covered by mangroves along the shores of tidal channels. The island has a tropical climate. Additionally, palaeotsunami deposits are preserved in swales in the beach ridge system along the western coast of Thailand (e.g. Jankaew et al. 2008; Gouramanis et al. 2017). Furthermore, although local beaches were lost in the 2004 tsunami, satellite photography showed recovery within 18 months (e.g. Choowong et al. 2009).

Although this study used tsunami sediment transport calculations for analysis, other uncertainties remain, such as the effects of artificial features on the calculations. Because of its natural topography with few artificial features, Phra Thong Island is a rare case that is useful for verifying tsunami sediment transport calculations with less uncertainty.

2.2. *Topography and bathymetry data*

Topography and bathymetry data used for the tsunami sediment transport calculations were created based on various water depths and elevations. Figure 2 shows the terrain data that were created. Topographic data were created from Region 1, which includes the Andaman Sea, to Region 6, which

https://doi.org/10.5194/nhess-2019-263
Preprint. Discussion started: 26 August 2019

Natural Hazards and Earth System Sciences
Discussions

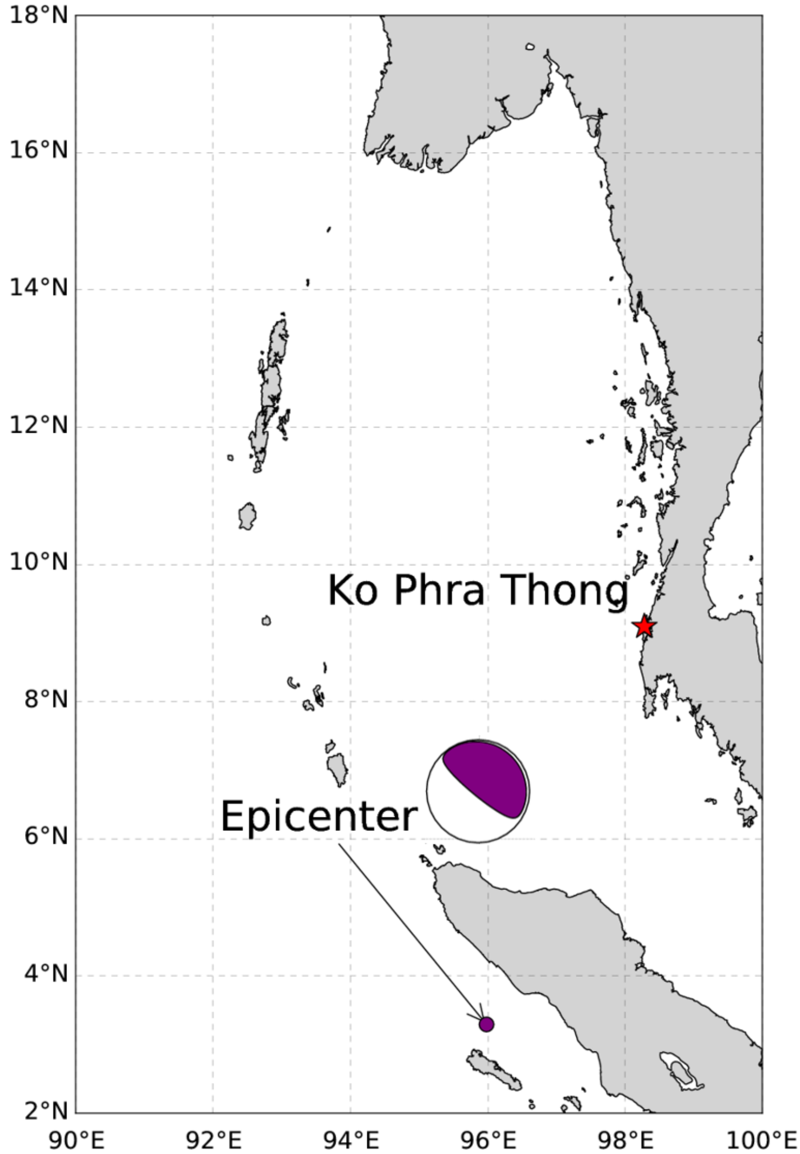

Figure 1 Location of Phra Thong Island

includes all of Phra Thong Island. The grid spacing from Region 1 to Region 6 is 1,215 m, 405 m, 135 m, 45 m, 15 m, and 5 m, respectively. In the tsunami sediment transport calculation, plane calculation was performed using an orthogonal coordinate system; the coordinate system of the target area Phra Thong Island is UTM 47N. Region 1 is the projection of depth data of the 30-second grid provided by GEBCO (2014) on the Cartesian coordinate system UTM 47N. Regions 2–4 use a digital marine chart with 300 m resolution based on a survey by the Thai Navy. Regions 5 and 6 use an original 5 m (terrain

https://doi.org/10.5194/nhess-2019-263
Preprint. Discussion started: 26 August 2019

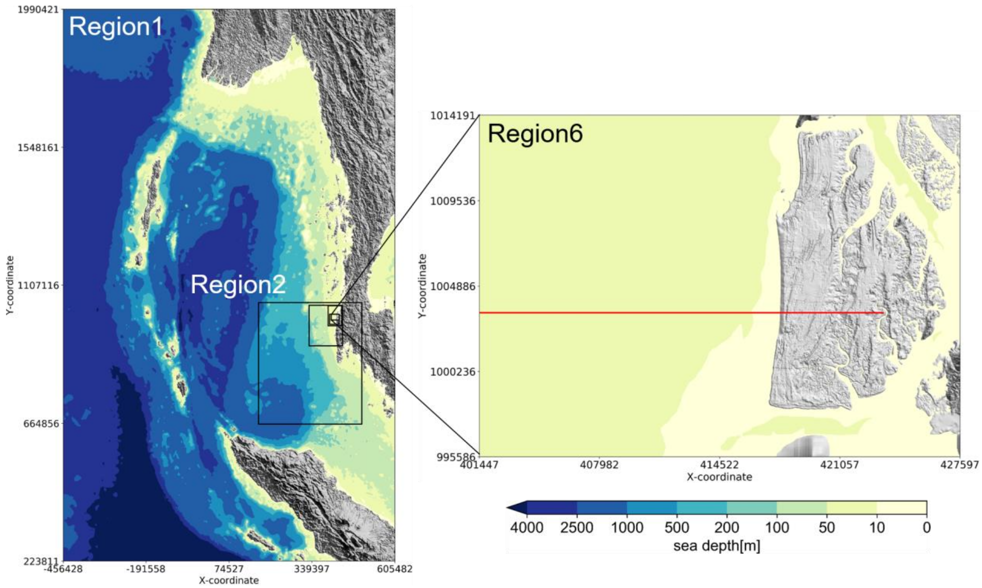

Figure 2 Terrain data (The black frame shows Region 1 to Region 6, and the red line in Region 6 shows the cross-section where calculation was performed.)

data) and 15 m (sea depth data) grid spacing to create mean terrain and water depth data based on analysis of satellite image by EOMAP and elevation data provided by the Land Development Department of Thailand. The terrain data of Region 4, created from the digital marine chart of 300 m resolution, showed discontinuity at the boundary with Region 5, which had a higher resolution. The discontinuity was therefore removed to the extent possible by interpolation with an inverse distance weighting method using all terrain data.

2.3. *Tsunami source model*

The fault model proposed by Suppasri et al. (2011) was used as the tsunami source of the 2004 Indian Ocean Tsunami. The fault model is divided into six small faults from satellite image analysis and survey results, and it is assumed that each small fault slides simultaneously and instantaneously. For the tsunami source, the vertical tectonic displacement in each fault was calculated according to Okada (1985). Table 1 shows the fault parameters of each fault and Figure 3 shows the initial water level.

https://doi.org/10.5194/nhess-2019-263
Preprint. Discussion started: 26 August 2019

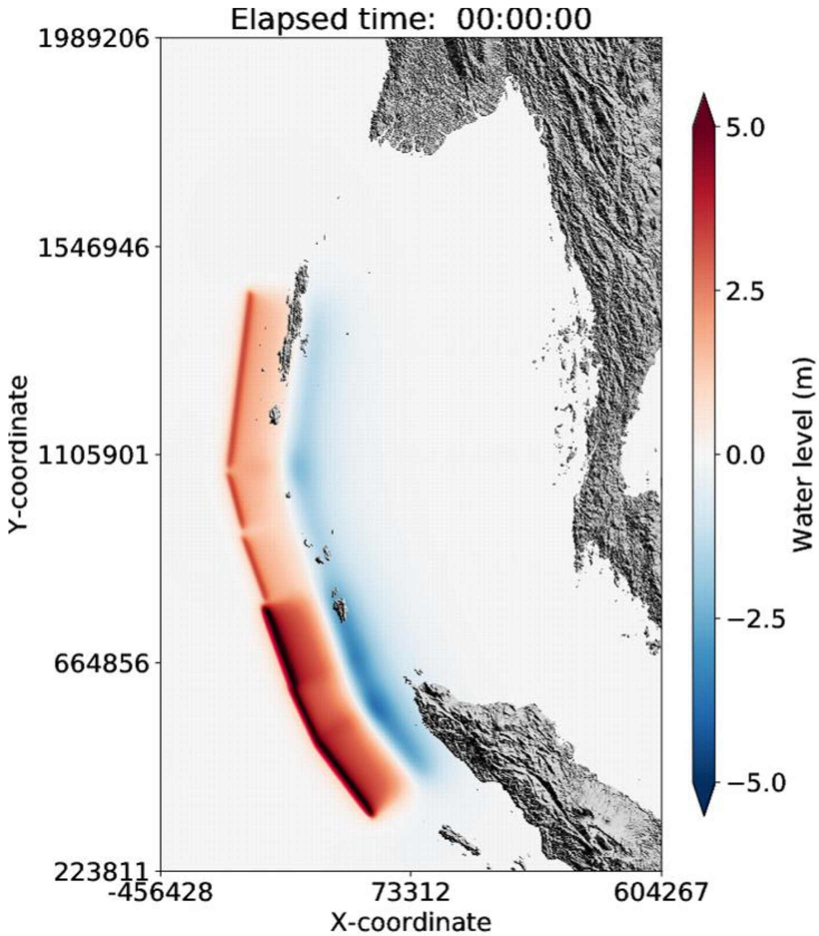

Figure 3 Initial water level

Table 1 Fault parameters (Suppasri et al., 2011)

Segment No.	1	2	3	4	5	6
Latitude(°N)	3.03	4.48	5.51	7.14	8.47	9.63
Longitude(°E)	94.40	93.32	92.87	92.34	91.88	91.57
Strike(deg)	323	335	340	340	345	7
Dip(deg)	15	15	15	15	15	15
Slip(deg)	90	90	90	90	90	90
Length(km)	200	125	180	145	125	380
Width(km)	150	150	150	150	150	150
Dislocation(m)	14	12.6	15.1	7	7	7
Depth(km)	10	10	10	10	10	10

2.4. *Tsunami sediment transport calculation*

2.4.1. *Tsunami propagation and run-up model*

Tohoku University's Numerical Analysis Model for Investigation of Near-field tsunamis, No. 2 (TUNAMI-N2) is based on the nonlinear long wave theory and was used as the tsunami propagation and run-up model.

$$\frac{\partial \eta}{\partial t}+\frac{\partial M}{\partial x}+\frac{\partial N}{\partial y}=0 \tag{1}$$

$$\frac{\partial M}{\partial t}+\frac{\partial}{\partial x}\left(\frac{M^2}{D}\right)+\frac{\partial}{\partial y}\left(\frac{MN}{D}\right)+gD\frac{\delta \eta}{\delta x}+\frac{gn^2}{D^{\frac{7}{3}}}M\sqrt{M^2+N^2}=0 \tag{2}$$

$$\frac{\partial N}{\partial t}+\frac{\partial}{\partial x}\left(\frac{MN}{D}\right)+\frac{\partial}{\partial y}\left(\frac{N^2}{D}\right)+gD\frac{\delta \eta}{\delta y}+\frac{gn^2}{D^{\frac{7}{3}}}N\sqrt{M^2+N^2}=0 \tag{3}$$

Here, η is the change in water level from the still-water surface, D is the total water depth from the bottom to the water surface, and g is the acceleration of gravity. The bottom friction is expressed according to the Manning formula, where n is Manning's roughness coefficient. M and N are the total flow fluxes in the x and y directions, respectively, and are given by integrating the horizontal flow velocity u, v from the water bottom h to the water surface η. It is assumed that the horizontal flow velocity is uniformly distributed in the vertical direction.

The nonlinear long wave theory consists of a continuous equation that is derived from (1) the principle of conservation of mass (continuity equation) and (2) the conservation of momentum (equation of motion). These two equations are obtained by vertically integration from the seabed to the water surface.

When the water depth is about 50 m or less, the effects of the 2nd, 3rd and 5th terms of the advection and seabed friction terms (Equations 2 and 3) are reduced, therefore wave theory that omit these terms is often used at depths shallower than 50 m. Meanwhile, the Message Passing Interface (MPI) parallel was implemented in the model for highly efficient calculations. Both the advection term and the bottom friction term were therefore considered in the calculations without reducing accuracy in deeper waters.

2.4.2. *Tsunami movable bed model*

For the tsunami movable bed model, we used the numerical sediment transport model (STM) proposed by Takahashi et al. (2000), which solves the time evolution of sediment transport considering the exchange sediment volume of the bed and suspended load layers according to the flow conditions of the nonlinear long wave theory-based TUNAMI-N2 model.

This model divides sediment transport by the tsunami into a bed load layer, where sediment grains pull,

Natural Hazards and Earth System Sciences Discussions

and a suspended load layer, where sediment grains float. The governing equations consist of continuous equations for the bed load layer and the suspended load layer, which are shown below.

$$\frac{\partial Z_B}{\partial t}+\frac{1}{1-\lambda}\left(\frac{\partial q_{B_x}}{\partial x}+\frac{\partial q_{B_y}}{\partial y}+\omega_{ex}\right)=0 \tag{4}$$

$$\frac{\partial \bar{C}_s M}{\partial x}+\frac{\partial \bar{C}_s N}{\partial y}-\omega_{ex}+\frac{\partial \bar{C}_s h_S}{\partial t}=0 \tag{5}$$

Equation (4) is a continuous equation for within the bed load layer. The first term is the exchange sediment volume with the bottom, the second term is the balance of sediment flow volume moving in a tractive form in the flow direction, and the third term defines the balance of suspension flux, caused by diffusion, and sedimentation flux, caused by gravity, as the exchange sediment volume between the bed load layer and the suspended load layer. ω_{ex} is expressed by the following equation.

$$\omega_{ex}=\epsilon_z\frac{\partial C}{\partial z}-\omega_0 C \tag{6}$$

Here, ρ_s is the sediment grain density, λ is the sediment grain porosity, Z_B is the bottom height from the reference plane, q_B is the amount of bed load sediment, ε_z is the diffusion coefficient in the vertical direction, C is the concentration in the vicinity of the boundary between the bed load layer and the suspended sediment layer, ω_0 is the sedimentation velocity of the sediment grains, C_B is the average bed load sediment concentration, h_B is the bed load layer thickness, C_S is the average suspended load layer concentration, h_s is the suspended load layer thickness, and M is the bed load flux. w_0 is the sedimentation velocity of the sediment grains. Equation (5) is a continuous equation for within the suspended load layer. The first and second terms are bed load sediment moving in a suspended state in the flow direction, the third term is the exchange sediment volume between the bed load layer and the suspended load layer, and the fourth term is the increase or decrease of the sediment flow in the suspended load layer.

In Equations (4) and (5), the equation defining the bed load sediment volume q_B and the equation defining the exchange sediment volume w_{ex} of the bed load layer and suspended load layer are necessary, but according to Takahashi et al. (1999), they are obtained by the following.

$$q_B=\alpha\sqrt{sgd^3}(\tau_*-\tau_c)^{\frac{3}{2}} \tag{7}$$

$$\omega_{ex}=\beta\sqrt{sgd}(\tau_*-\tau_c)^2-\omega_0\bar{C}_s \tag{8}$$

$$\tau_* = \frac{u_*^2}{sgd} \tag{9}$$

Here, α is the coefficient of the bed load sediment volume equation, β is the coefficient of the suspension volume equation, s is specific gravity in water, g is the acceleration of gravity, d is grain diameter, τ_* is the Shields number, τ_c is the limit Shields number, u_* is the friction velocity obtained from the Manning formula.

In the model comprised of Equation (4) and Equation (5), the bottom height Z_B from the reference plane and the average suspended sediment concentration C_S are the initial values before the tsunami and the flow flux M, respectively. Because suspended sediment thickness h_S is given by the equation of motion of a fluid and the continuous equation, sea level fluctuation can be determined over time. Further, the MPI parallel was implemented according to Yamashita et al. (2016) in this model to enable relatively efficient wide area calculations.

2.5. *Calculation conditions*

Here we explain the conditions for the numerical calculations. Figure 3 was used for the tsunami source, while Figure 2 was used for terrain data. The calculations were performed using a 3:1 nested grid that increased the resolution a 1215 m grid to a 5 m grid. Additionally, the target region of the sediment transport calculation was limited to Region 6, with a grid spacing of 5 m.

The simulations were calculated over a 0.05 second increment with a 6 hour period in which the suspended sediment concentration in the vicinity of the shoreline decreased and stabilized. For the bottom conditions, the Manning's roughness coefficient was fixed at n = 0.025, and the entire area of Region 6 was considered the movable bed. The grain size was based on one sediment data set (Gouramanis et al., 2017) from the locally eroded region, and was considered as a representative value for all of the tsunami sediment grain sizes. A uniform grain size of D_{50} = 0.127 mm was used.

The limit Shields number τ_c in Equations (7) and (8) was obtained using Equations (10) and (11) according to Iwagaki et al. (1954), as shown below.

$$\tau_c = u_c^2 \rho \tag{10}$$

$$u_c^2 = 8.41 d^{\frac{11}{32}} \tag{11}$$

Here, u_c is the friction velocity and ρ is the density of water.
Table 2 shows each parameter set used for sediment transport calculations in this study.

https://doi.org/10.5194/nhess-2019-263
Preprint. Discussion started: 26 August 2019

Table 2 Set parameters for sediment transport calculations

Variable	Set Value
Coefficient of bed load sediment volume equation α	6.55
Coefficient of suspension sediment volume equation β	9.1×10^{-5}
Friction speed u_c	0.01353 m/s
Bottom slope correction factor ε	2.5
Sedimentation velocity of sediment grains w_0	0.1353 m/s
Maximum suspended sediment concentration C_{max}	37.7%
Specific gravity of sediment grains in water s	1.65
Void ratio λ	0.4

3. Result

3.1. *Verification of reproducibility*

3.1.1. *Tsunami trace height*

The reproducibility of the calculated results is based on the tsunami trace height data (IUGG; available at http://www/nda.ac.jp/fu-jima/TMD/index.html) for the 2004 Indian Ocean Tsunami is discussed using geometric mean K and geometric standard deviation κ proposed by Aida (1978). Figure 4 shows results of calculation of the maximum inundation depth of trace height data at seven available sites on Phra Thong Island. The geometric mean K and the geometric standard deviation κ can also be obtained using the following formula (Aida, 1978).

$$\log K = \frac{1}{n}\sum_{i=1}^{n} \log K_i \tag{12}$$

$$\log\kappa = \sqrt{\frac{1}{n}\left\{\sum_{i=1}^{n}(\log K_i)^2 - n(\log K)^2\right\}} \tag{13}$$

Here, n is the number of points, R_i is the trace height at the ith point, H_i is the calculated value at the ith point, and $K_i = R_i/H_i$. From Equations (12) and (13), $K = 0.96$ and $\kappa = 1.10$ are obtained. Additionally, the source model used in this calculation gives $K = 0.84$ and $\kappa = 1.30$ for reproducibility of tsunami trace height in the wide area along the coast of Thailand (Suppasri et al., 2011). The Japan Society of Civil Engineers (2012) consider $0.95 < K < 1.05$ and $\kappa < 1.45$ as guides for evaluating reproducibility of tsunami numerical calculations. Therefore, it can be said that this calculation has good tsunami reproducibility.

https://doi.org/10.5194/nhess-2019-263
Preprint. Discussion started: 26 August 2019

Natural Hazards and Earth System Sciences
Discussions

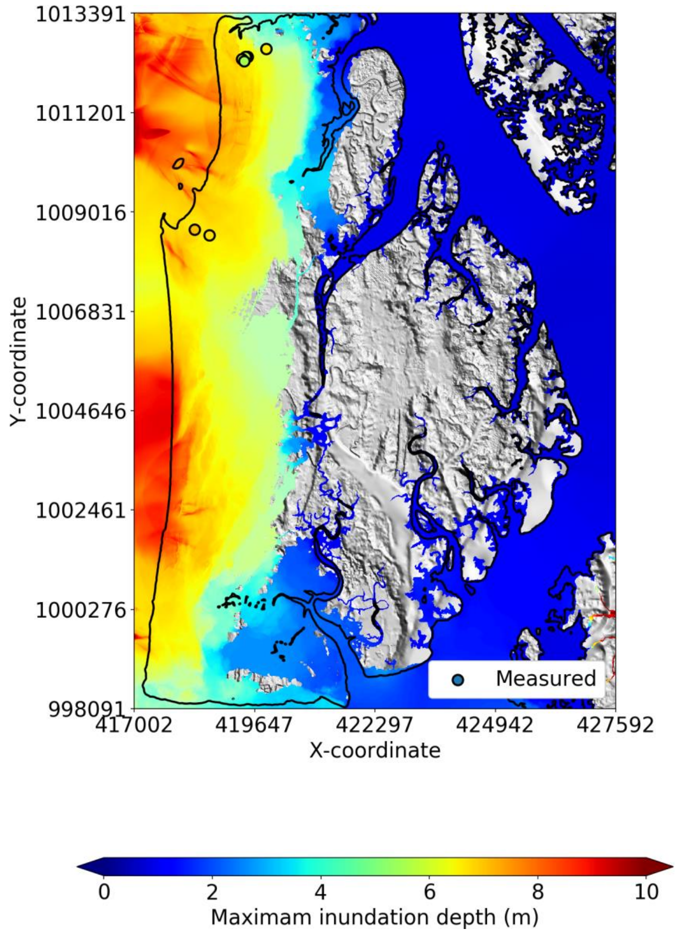

Figure 4 Comparison of calculated and measured maximum inundation depth

3.1.2. *Change of shoreline*

Our sediment transport models reproduce the locations of sediment erosion and these are confirmed from satellite images. First, Figure 5 shows topographical changes caused by the tsunami and the shoreline before (dashed line) and after (solid line) the tsunami in this calculation. As shown in Figure 5, local erosion was largely observed in regions (a) and (b)..Comparison with the satellite image shows that the position of erosion in both regions is consistent (Figure 6). Although the actual amount of erosion is unknown, this indicates that the planar spread of the eroded part can be relatively well reproduced relatively by the calculation. Region (a) was further investigated in detailed as the area corresponds to the point where sediment outflow was confirmed by Jankaew et al. (2008) in the following section.

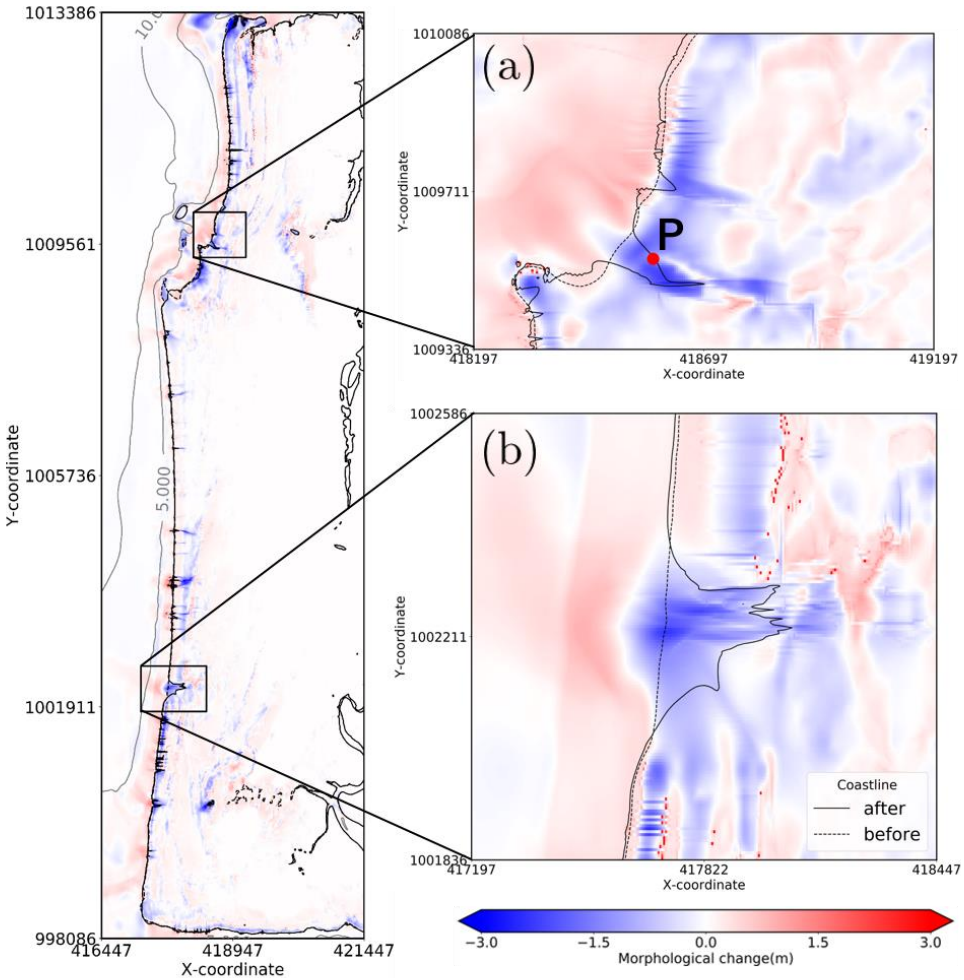

Figure 5 Topographic change and shoreline position immediately after the tsunami

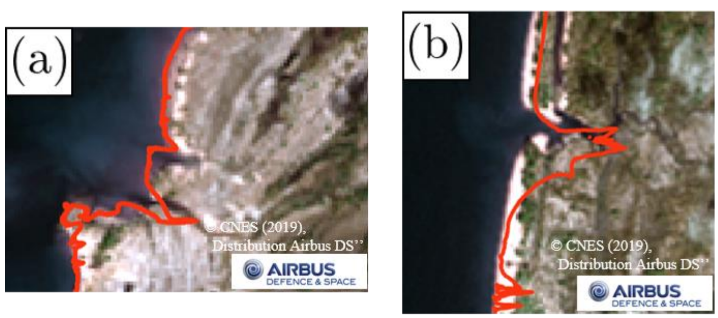

Figure 6 Comparison of shoreline position in satellite image and calculation results (© CNES, 2019, Distribution Airbus DS'')

https://doi.org/10.5194/nhess-2019-263
Preprint. Discussion started: 26 August 2019

Natural Hazards and Earth System Sciences
Open Access
Discussions

3.1.3. *Sediment layer*

Here we discuss the distribution of sediment thickness from the sediment transport models based on sediment data from prior studies. Figure 7 compares sediment layer thickness in this calculation with sediment data from 148 points (Jankaew et al., 2008; Gouramanis et al., 2017).

Although the calculated value of sediment thickness is slightly overestimate in general, Figure 7 shows that the inland thinning tendency is reproducible. Because overestimation is a result of considering the entire area as a movable bed in the calculation, ground which is not easily eroded in reality may appear excessively eroded.

The grain size in this calculation is based on using sediment data (Gouramanis et al., 2017) from one point in region (a) of Figure 5 as a representative value of the entire area. It is possible that the grain size may not be representative of the sediment within region (a). Therefore, Figure 8 shows the result of calculations with the larger grain size D_{50} = 0.3 mm as a representative value.

Figure 8 confirms the improved reproducibility through smaller variation of calculation results compared with D_{50} = 0.127 mm. Future studies should consider that the grain size considered representative in region (a) may not be representative of the wider area, and further sediment grain size analysis of the 2004 IOT sediment deposits from elsewhere on the island may improve tsunami sediment transport modelling onto the island.

In addition, Figures 7 and 8 confirm that tsunami inundation of Phra Thong Island exceeded 2,000 m, and the grain size had no influence to the simulated inundation distance. In areas where the inundation distance exceeded 2,000 m, i.e. near the inundation limit and along the large tidal channels in the east, the measured tsunami deposits of 10 cm or more exist could not be reproduced by the simulation. There are two possible reasons for this. (1) In the Great East Japan Earthquake tsunami, sandy sediments were deposited up to 57–76% of the inundation limit, and muddy sediments were deposited further inland (Goto et al., 2011b; Goto et al Abe et al., 2012; Chague´–Goff et al., 2012). The same phenomenon may therefore have occurred. However, there is not much mud in this system. The beach ridges are mostly medium to coarse sand as is the nearshore and offshore environment. Therefore, this assumption may not be applicable to Phra Thong Island (2) It is possible that the tsunami eroded sediment within the tidal channels as the tsunami flowed out of these channels. This suggests that finer grain sizes were deposited beyond 2,000 m of the western coast.

3.2. *Sediment transport process*

Figure 5 shows the local erosion caused by the sediment transport processes in region (a). The calculated time series changes of water level and ground height at point P in region (a) are shown in Figure 9. It is apparent from Figure 9 that the first wave arrived 2 hours 40 minutes after the earthquake, and backwash was generated 10 minutes later. At Point P. the ground elevation increased by about 50 cm through sediment deposition during the first inflowing wave and was largely eroded during the backwash, so beach loss in region (a) is considered to be a result of erosion during the backwash.

https://doi.org/10.5194/nhess-2019-263
Preprint. Discussion started: 26 August 2019

Natural Hazards and Earth System Sciences
Open Access
Discussions

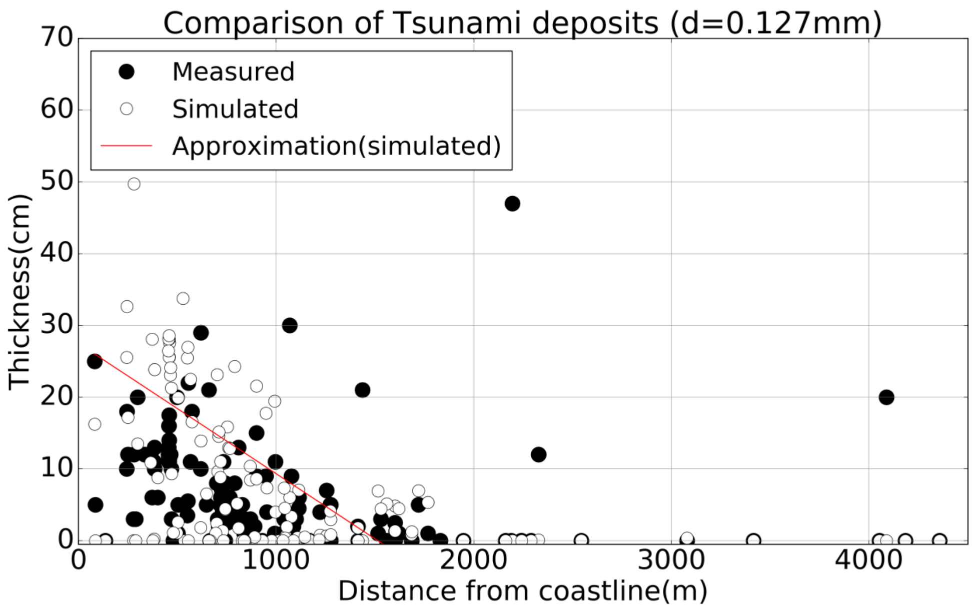

Figure 7 Comparison of tsunami deposit thickness with representative grain size D_{50} = 0.127 mm (calculated value and measured value)

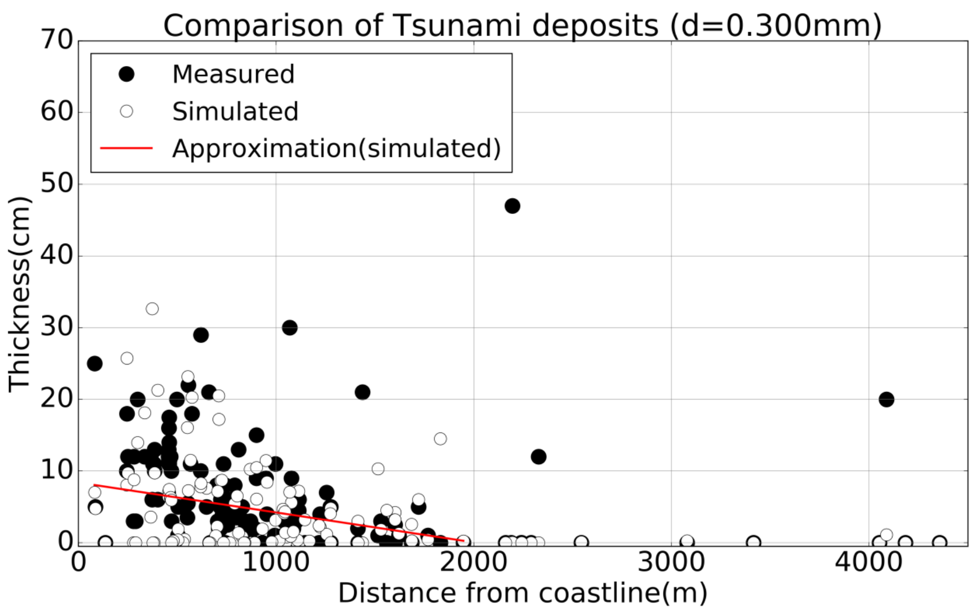

Figure 8 Comparison of tsunami deposit thickness with representative grain size D_{50} = 0.300 mm (calculated value and measured value)

https://doi.org/10.5194/nhess-2019-263
Preprint. Discussion started: 26 August 2019

Natural Hazards and Earth System Sciences
Open Access
EGU
Discussions

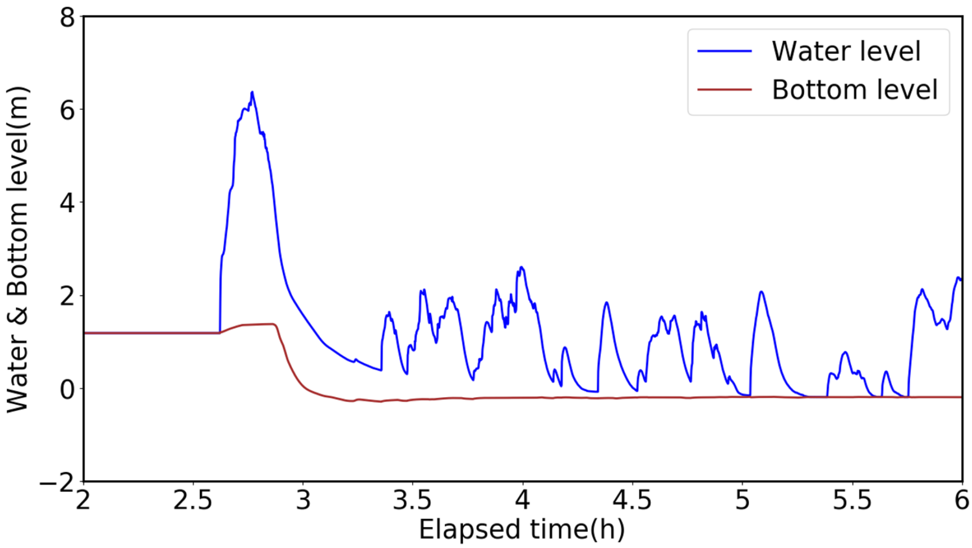

Figure 9 Chronological change of water level and ground height at point P in region (a)

Additionally, based on the waveform (which assumes a flat surface), a cross section calculation was carried out along the survey line in Figure 2. Figure 10 shows the chronological changes in ground height, water level, suspended sediment concentration and saturation of suspended sediment concentration on the survey line at each unit of time. As shown in Figure 10, seabed erosion was observed at a depth of about 20 m or less during the first inflowing wave because of increased suspended sediment concentration and decreased of sea depth. The eroded sediment was transported into the shallow water area thereafter, and the concentration of suspended sediment far exceeded the saturation of suspended sediment concentration in the vicinity of the shoreline. Sedimentation was therefore considered predominant near the shoreline. In other words, it is estimated that sediment eroded in the shallow water area during the first lead wave, and much sediment was transported inland. After the run-up, suspended sediment concentration decreased, and most of the sediment that eroded in the shallow water area was deposited near the shoreline, while the remainder was transported inland. Inland, it was found that erosion and deposition occurred according to topographical conditions.

During the backwash, the suspended sediment concentration near the shoreline rises as the backwash progresses offshore, thus the beach near the shoreline was eroded by the backwash and flowed out to sea.

4. Discussion

4.1. *Sediment transport process and beach recovery factors*

Region (a) in Figs 5 and 6 were selected for detailed investigation of the simulation results and discussion. In the sediment transport process on Phra Thong Island, a tsunami wave large enough to

https://doi.org/10.5194/nhess-2019-263
Preprint. Discussion started: 26 August 2019

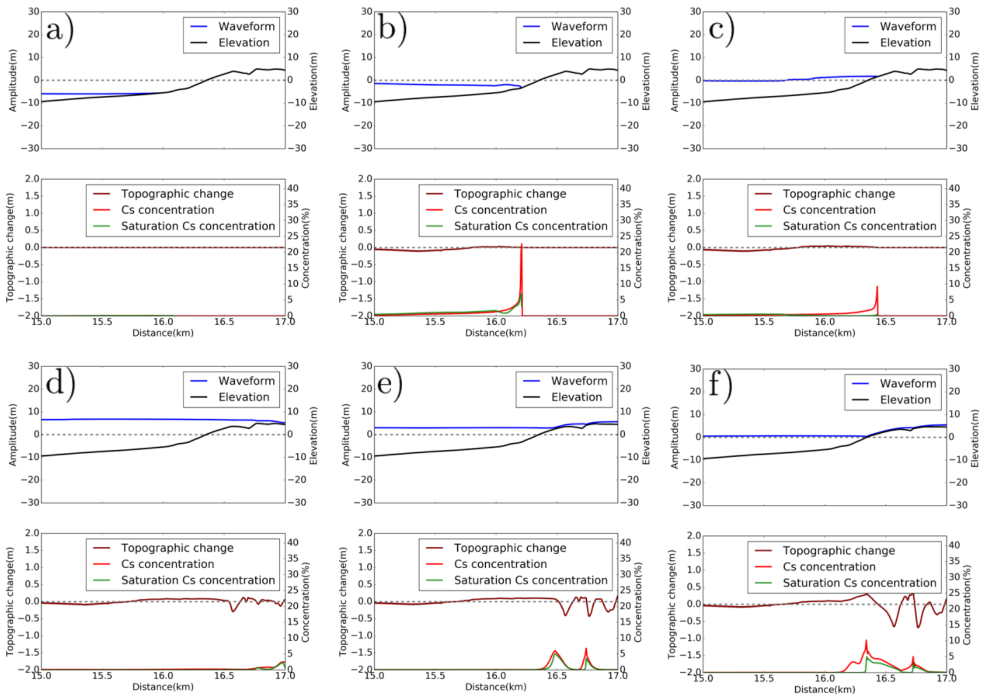

Figure 10 Change in water level, flow velocity, ground height, suspended sediment concentration, and saturation suspended sediment concentration by section calculation along the survey line in (a) 1st backwash, b) Prior to 1st leading wave run-up, c) Start of 1st leading wave run-up, d) Advance of 1st leading wave run-up, e) Start of 2nd backwash, f) Advance of 2nd backwash

expose the nearshore sediments ran up the exposed nearshore area while retaining sediment from the shallow water. The sediment concentration gradually increases while running up the relatively long distance of the exposed nearshore, and became sediment-saturated as the wave reached the shoreline, making it difficult for new sediment to be eroded further. This can explain why the degree of beach erosion is small during the leading wave, and may be a characteristic sediment transport property of shallow beaches like those on Phra Thong Island. In other words, numerical simulation results suggest that there is little transportation of sediments from the shoreline by the first inflowing wave and that inland deposits were formed by sediment transported from the sea. Similarly, analysis of microfossils (Sawai et al., 2009) from preserved 2004 IOT tsunami deposits inland suggests that tsunami deposits on Phra Thong Island originated from shallow nearshore zone. Pham et al. (2018) suggested that sediment grain sizes and mineralogy were most similar to those of nearshore sediments, but that geochemically the 2004 IOT sediments were a combination of nearshore and onshore sources, but that quantifying the contributions from different environments remains a challenge. The sediment transport modelling suggests that most sediment comes from the shallow offshore and nearshore environment. Figure 11 shows the results of the calculated sediment deposition onshore and offshore Phra Thong

https://doi.org/10.5194/nhess-2019-263
Preprint. Discussion started: 26 August 2019

Natural Hazards and Earth System Sciences
Open Access
Discussions

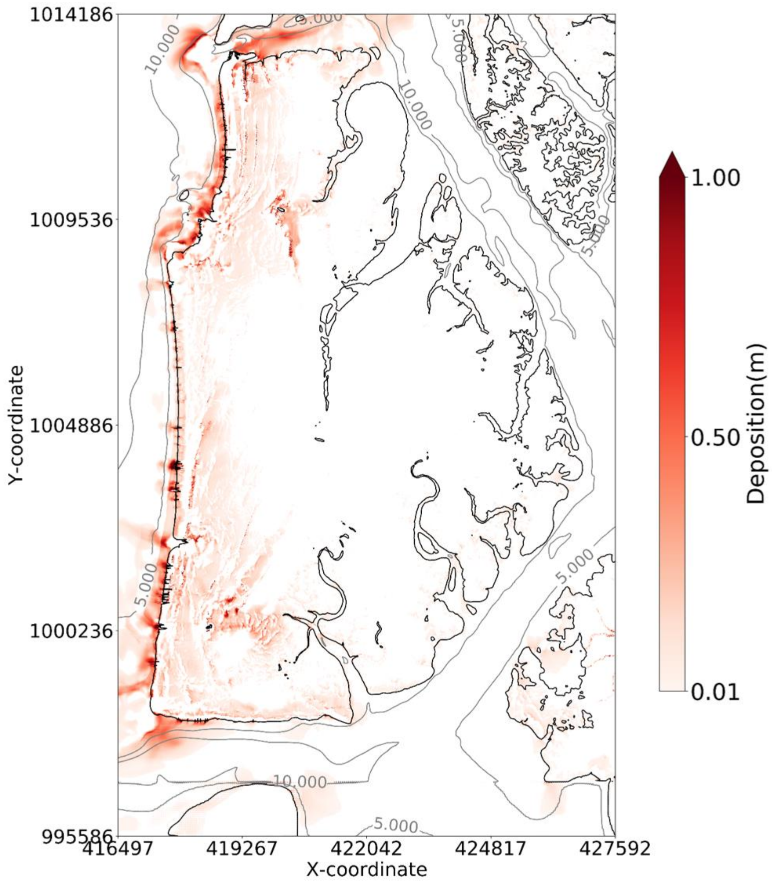

Figure 11 Sediment distribution (showing depth contours at 5 m intervals in the sea area)

Island. From the modelling results, most of the eroded sediment in region (a) was deposited in shallow nearshore environments in water less than approximately 5 m deep.

Therefore, the calculations show that the sediment that flowed from the lost beach was deposited in relatively shallow water, which would facilitate rapid recovery of the coastal environment shortly after the tsunami, when normal coastal conditions return. This study considered only sediment transport and topographic change caused by the tsunami to determine the initial condition of the recovery process. However, our results show that sediment flowing out from the beach were deposited in relatively shallow water, allowing for rapid sediment transport to the shoreline in subsequent coastal conditions. Future studies can build on these findings to determine the offshore extent of sediment transport and deposition, and identify the processes of coastal recovery on Phra Thong Island. The erosion of the beaches changed the sediment budget significantly, with large volumes of sediment relocated into the nearshore. The removal of sediment from the coastal zone also generated accommodation space which was rapidly infilled upon normal wave and tidal conditions.

Geomorphologically, the Sendai Plain, which was inundated by the March 11, 2011 Great East Japan tsunami, is similar to the beach ridge plain on Phra Thong Island (refs needed), but most of the tsunami sediment deposited onshore came from terrestrial sources (Goto et al., 2012; Szczucin´ski et al., 2012; Takashimizu et al., 2012; Sugawara et al., 2014). However, the Great East Japan tsunami differed from the 2004 IOT as the Japanese event had a much smaller receding wave (Nationwide Ocean Wave information network for Ports and HArbourS, NOWPHAS). As such the Japanese tsunami may not have achieved sediment saturation as the wave approached the shoreline, thereby containing a lower sediment concentration and allowing large volumes of sediment to be entrained from the beach for subsequent formation of inland deposits. The different sources of deposited sediment in the two areas reflects contrasting characteristic sediment transport properties on shallow beaches, and may be useful for estimating paleotsunami from coast recovery and geological records.

4.2. *Limits of calculation results*

This study analyzed tsunami sediment transport on Phra Thong Island using numerical calculations and assumed that the island was unvegetated and lacked topography. However, the western half of the island has an undulating surface caused by the beach ridge and swale system, and is extensively vegetated with trees and dense grasses on the ridges and thick grasses within the swales. The eastern half of the island has wide tidal channels and an extensive fringing mangrove system. Both topography and differing vegetation types add complexity to the inundation and backflow sediment transport models not captured here. In future, it is necessary to consider the influence of vegetation on tsunami sediment transport.

Another potential limitation of the model is the selection of a single (median) grain size for the sediments. As shown in previous studies(e.g. Sugawara et al., 2014a), the assumption of transport of single grain sized sediment differs from actual situations because of the distribution of grain sizes mobilised and deposited by tsunami. Therefore, it is important to set representative grain sizes and fully study how grain size affects tsunami sediment transport. Future modelling may consider simulating the suite of grain sizes individually or simulating a population of grain sizes that are identified in the modern environment and in preserved tsunami deposits.

Furthermore, although the calculation was performed considering the entire area a movable bed, the existence of fixed beds, such as rocky areas, should be considered. We consider this a minor component of this research as the rocky headlands that serve as fixed beds are relatively small in area and would contribute little to the overall simulations in our models.

Sugawara et al. (2014b) considers the simulation result of sediment layer thickness using the tsunami sediment transport calculation to be affected by grain size, bottom conditions and topographic data. Their study showed that the layer thickness increases as grain size becomes finer and the layer thickness distribution tendency was unchanged regardless of grain size. Similar results were obtained in this study. Additionally, because bottom surface roughness greatly affects sediment transport near the shoreline, varying bottom surface conditions may influence future modelling results on Phra Thong Island.

5. Conclusion

Because of insufficient knowledge about the topographic recovery process after a tsunami, this study used sediment transport modelling to identify the erosional and depositional processes affecting the beach at Phra Thong Island, Thailand during the 2004 Indian Ocean Tsunami.

First, it was confirmed by comparing the measured and calculated values of the sediment layer thickness that the location of beach runoff identified on Phra Thong Island was reproducible and consistent with sediment transport results. Based on the sediment transport results we conclude that the processes of sediment erosion and deposition on Phra Thong Island are characterized by the following sequence:

- erosion caused by the inflowing waves occurred at a relatively shallow location in the offshore area and the transported sediment was deposited near the shoreline;
- the inflowing waves caused minimal erosion of the shoreline;
- onshore sediment deposition is due to onshore topographical features trapping sediments prior to backwash; and,
- erosion of the shoreline was largely caused by backwash resulting in onshore sediments deposited in the shallow nearshore zone.

Rapid beach recovery on Phra Thong Island is facilitated due to the large volume of sediment deposited in the nearshore zone and the large accommodation space available for remobilization and redeposition of sediments when normal coastal conditions resume soon after the tsunami causing a re-equilibration of the beach.

6. Acknowledgements

We would like to express our gratitude for the support and data received from Panon Latcharote of the Faculty of Science and Technology of Thammasat University as well as help and support from Prof. Dr. Supot Teachavorasinskun, Dean of Faculty of Engineering, Chulalongkorn University; and the Royal Thai Navy. RM, AS, KY, FI was support by JSPS Grant-in-Aid for Scientific Research (A) No. 17H01631 (FY2017 - FY2021). AS and NL was support by JSPS Bilateral program for joint research with National Research Council of Thailand (NRCT) (FY2017 - FY2018). CG was supported by NUS start-up grant (R-109-000-223-133). NL was supported by Ratchadapisek Sompoch Endowment Fund (2019), Chulalongkorn University (762003-CC). This work is a contribution to IGCP Project 639, 'Sea-level Change from Minutes to Millennia'.

References

1) Abe, T., Goto, K., and Sugawara, D.: Relationship between the maximum extent of tsunami sand and the inundation limit of the 2011 Tohoku–oki tsunami on the Sendai Plain, Japan, Sedimentary Geology, 282, 142–150, 2012.
2) Aida, I.: Reliability of a tsunami source model derived from fault parameters, J. Phys. Earth, 26, 57–73, 1978.

https://doi.org/10.5194/nhess-2019-263
Preprint. Discussion started: 26 August 2019

Natural Hazards and Earth System Sciences
Open Access
EGU
Discussions

3) Yunus Ali, P., and Narayama, A. C.: Short–Term Morphological and Shoreline Changes at Trinkat Island, Andaman and Nicobar, India, After the 2004 Tsunami, Marine Geodesy, 38, 26–39, 2015.

4) Brill, D., Klasen, N., Jankaew, K., Brückner, H., Kelletat, D., Scheffers, A., and Scheffers, S.: Local inundation distances and regional tsunami recurrence in the Indian Ocean inferred from liminescence dating of sandy deposits in Thailand, Natural Hazards and Earth System Sciences, 12, 2177–2192, 2012.

5) Brill, D., Klasen, Brückner, H., Jankaew, K., Scheffers, A., Kelletat, D., and Scheffers, S.: OSL dating of tsunami deposits from Phra Thong Island, Thailand, Quaternary Geochronology, 10, 224–229, 2012.

6) rill, D., Jankaew, K., Bruckner, H.: Holocene evolution of Phra Thong's beach-ridge plain (Thailand) — Chronology, processes and driving factors, Geomorphology, 245, 117–134, 2015.

7) ChaguéGoff, C., Andrew, A., Szczuciński, W., Goff, J., and Nishimuira, Y.: Geochemical signatures up to the maximam inundation of the 2011 Tohoku–oki tsunami — Implications for the 869 AD Jogan and other palaeotsunamis, Sedimentary Geology, 282, 65–77, 2012.

8) Choowong, M., Phantuwongraj, S., Charoentitirat, T., Chutakositkanon, V., Yumuang S., and Charusiri, P.: Beach recovery after 2004 Indian Ocean tsunami from Phang–nga, Thailand, Geomorphology, 104, 134–142, 2009.

9) Fagherazzi, S. & Du, X.: Tsunamigenic incisions produced by the December 2004 earthquake along the coasts of Thailand, Indonesia and Sri Lanka, Geomorphology, 99, 120–129, 2008.

10) Fujino S., Naruse H., Matsumoto, D., Jarupongsakul T., Sphawajruksakul A., and Sakakura, N.: Stratigraphic evidence for pre–2004 tsunamis in southwestern Thailand, Marine Geology, 262, 25–28, 2009.

11) Fujino, S., Naruse, H., Matsumoto, D., Sakakura, N., Suphawajruksakul, A., and Jarupongsakul, T.: Detailed measurements of thickness and grain size of a widespread onshore tsunami deposit in Phang–nga Province, southwestern Thailand, Island Arc, 19, 389–398, 2010.

12) Goto, K., Takahashi, J., Oie, T., and Imamura, F.: Remarkable bathymetric change in the nearshore zone by the 2004 Indian Ocean tsunami: Kirinda Harbor, Sri Lanka, Geomorphology, 127, No.1-2, 107–116, 2011a.

13) Goto, K., ChaguéGoff, C., Fujino, S., Goff, J., Jaffe B., Nishimura, Y., Richmond, B., Sugawara, D., Szczuciński, W., Tappin, R. D., Witter, C. R., and Yuliant, E., New insights of tsunami hazard from the 2011 Tohoku–oki event, Marine Geology, 290, 46–50, 2011b.

14) Goto, K., Chague´Goff, C., Goff, J., and Jaffe, B.: The future of tsunami research following the 2011 Tohoku–oki event, Sedimen- tary Geology, 282, 1–13, 2012.

15) Gouramanis, C., Switzer, A. D., Polivka, P. M., Bristow, C. S., Jankaew, K., Dat, P. T., Pile, J., Rubin, C. M., Yingsin, L., Ildefonso, S. R., and Jol, H. M.: Ground penetrating radar examination of thin tsunami beds - A case study from Phra Thong Island, Thailand,Sediment. Geol., 329, 149–165, 2015.

16) Gouramanis, C., Switzer, A. D., Jankaew, K., Bristow, C. S., Pham, D. T., and Ildefonso, S. R.:

High-frequency coastal overwash deposits from PHRA thong Island, Thailand, Sci. Rep., Vol.7, No. September 2016, 1–9, 2017.

17) Haraguchi, T., Takahashi, T., Hisamatsu, R., Morishita, Y., and Sasaki, I.: A Field Survey of Geomorphic Change on Kessennuma Bay caused by the 2010 Chilean Tsunami and the 2011 Tohoku Tsunami, Journal of JSCE, B2 (Coastal Engineering), 68, 231–235, 2012.

18) Hawkes, A.D., Bird, M., Cowie, S., Grundy-Warr, C., Horton, B.P., Hwai, A.T.S., Law, L., Macgregor, C., Nott, J., Ong, J.E., Rigg, J., Robinson, R., Tan-Mullins, M., Sa, T.T., Yasin, Z., Aik, L.W.: Sediments deposited by the 2004 Indian Ocean Tsunami along the Malaysia–Thailand Peninsula, Marine Geology, 242, 169–190, 2007.

19) Hirao, R., Tanaka, H., Umeda, M., Adityawan, M. B., Mano, A., and Udo, K.: Breaching of Sandy Coast and Spit Due To The 2011 Tsunami and Their Recovery, Journal of JSCE, B2(Coastal Engineering), 68, 581–585, 2012.

20) Imai, K., Sugawara, D., Takahashi, T., Iwama, S., and Tanaka, H.: Numerical study for sediment transport due to tsunami around the Kitakami River mouth, Journal of JSCE, B2(Coastal Engineering), 71, 247–252, 2015.

21) Iwagaki, Y.: Hydrodynamical study on critical tractive force, Trans. JSCE, 41(41), 1–21, 1956.

22) Jankaew, K., Atwater, B. F., Sawai, Y., Choowong, M., Charoentitirat, T., Martin, M. E., and Prendergast, A.: Medieval forewarning of the 2004 Indian Ocean tsunami in Thailand, Nature, 455(7217), 1228–1231, 2008.

23) Koiwa, N., Takahashi, M., Sugisawa, S., Ito, A., Aki Matsumoto, H., Tanavud, C., and Goto, K.: Barrier spit recovery following the 2004 Indian Ocean tsunami at Pakarang Cape, southwest Thailand, Geomorphology, 306, 314–324, 2018.

24) Liew, S.C., Gupta, A., Wong, P.P., Kwoh, L.K.: Recovery from a large tsunami mapped over time: The Aceh coast, Sumatra, Geomorphology, 114, 520–529, 2010.

25) Saegusa, S., Tanaka, H., and Mitobe, Y.: Recovery processes of bathymetry of Sendai Bay after the 2011 tsunami, Journal of JSCE, B2(Coastal Engineering), 73, 817–822, 2017.

26) Okada, Y.: Surface deformation due to shear and tensile faults in a half-space, Bulletin of the Seismological Society of America, 75(4), 1135–1154, 1985.

27) Pari, Y., Ramana Murthy, M. V., Jaya Kumar, S., Subramanian, B. R., and Ramachandran, S.: Morphological changes at Vellar estuary, India — Impact of the December 2004 tsunami, Journal of Environmental Management, 89, 45–57, 2008.

28) Paris, R., Lavigne, F., Wassmer, P., Sartohadi, J.: Coastal sedimentation associated with the December 26, 2004 tsunami in Lhok Nga, west Banda Aceh (Sumatra, Indonesia), Marine Geology, 238, 93–106, 2007.

29) Pham, T. D., Gouramanis, C., Switzer, M. A., Rubin, M. C., Jones, G. B., Jankaew, K., and Carr, F. P.: Elemental and mineralogical analysis of marine and coastal sediments from Phra Thong Island, Thailand: Insights into the provenance of coastal hazard deposits, Marine Geology, 385, 274–292, 2018.

30) Prendergast, L. A., Cupper L. M., Jankaew, K., and Sawai, Y.: Indian Ocean tsunami recurrence from optical dating of tsunami sand sheets in Thailand, Marine Geology, 295–298, No.15, 20–27, 2012.

31) Sawai, Y., Jankaew K., Martin, E. M., Prendergast, A., Choowong, M., and Charoentitirat, T.: Diatom assembles in tsunami deposits associated with th 2004 Indian Ocean tsunami at Phra Thong Island, Thailand, Marine Micropaleontology, 73, 70–79, 2009.

32) Sugawara, D., Goto, K., and Jaffe, B. E.: Numerical models of tsunami sediment transport –Current understanding and future directions, Marine Geology，352，295–320, 2014a.

33) Sugawara, D., Takahashi, T., and Imamura, F.: Sediment transport due to the 2011 Tohoku-oki tsunami at Sendai: Results from numerical modeling, Mar. Geol., 358, 18–37, 2014b.

34) Suppasri, A., Koshimura, S., and Imamura, F.: Developing tsunami fragility curves based on the satellite remote sensing and the numerical modeling of the 2004 Indian Ocean tsunami in Thailand, Nat. Hazards Earth Syst. Sci., 11(1), 173–189, 2011.

35) Switzer, A.D., Srinivasalu, S., Thangadurai, N., Ram Mohan, V.: Bedding structures in Indian tsunami deposits that provide clues to the dynamics of tsunami inundation, Geological Society, London, Special Publications, 361, 61-77, 2012.

36) Szczuciński, W., Kokociński, M., Rzeszewski, M., Chahué–Goff, C., Cachão, M., Goto, K., and Sugawara, D.: Sediment sources and sedimentation processes of 2011 Tohoku–oki tsunami deposits on the Sendai Plain, Japan — Insights from diatoms, nannoliths and grain size distribution, Sedimentary Geology, 282, 40–56, 2012.

37) Takahashi, T., Shuto, N., Imamura, F., and Asai, D.: Modeling sediment transport due to tsunamis with exchange rate between bed load layer and suspended load layer, Proceedings Of International Conference of Coastal Engineering，1508–1519, 2000.

38) Takahashi, T., Kurokawa, T., Fujita, M., and Shimada, H.: Hydraulic experiment on sediment transport due to tsunamis with various sand grain size, Journal of JSCE, B2(Coastal Engineering), 67, 231–235, 2011.

39) Takashimizu, Y., Urabe, A., Suzuki, K., and Sato, Y.: Deposition by the 2011 Tohoku–oki tsunami on coastal lowland controlled by beach ridges near Sendai, Japan, Sedimentary Geology, 282, 124–141, 2012.

40) Tanaka, H., Mano, A., and Udo, K.: Beach Morphology Change Induced by The 2011 Great East Japan Earthquake Tsunami, Journal of JSCE, B2(Coastal Engineering), 67(2), 571–575, 2011.

41) Udo, K., Tanaka, H., Mano, A., and Takeda, Y.: Beach Morphology Change of Southern Sendai Coast due to 2011 Tohoku Earthquake Tsunami, Journal of JSCE, B2(Coastal Engineering), 69, 391–395, 2013.

42) Udo, K., and Takeda, Y.: Comparison between characteristics of shoreline changes due to the 2004 Indian Ocean tsunami and the 2011 Great East Japan tsunami, Journal of JSCE, B3(Coastal Engineering), 72, 175–180, 2016.